Cell Reports
Resource

The Rac-FRET Mouse Reveals Tight Spatiotemporal Control of Rac Activity in Primary Cells and Tissues

Anna-Karin E. Johnsson,[1,4] Yanfeng Dai,[1,4,5] Max Nobis,[2] Martin J. Baker,[1] Ewan J. McGhee,[2] Simon Walker,[1] Juliane P. Schwarz,[2] Shereen Kadir,[2] Jennifer P. Morton,[2] Kevin B. Myant,[2] David J. Huels,[2] Anne Segonds-Pichon,[1] Owen J. Sansom,[2] Kurt I. Anderson,[2] Paul Timpson,[2,3,*] and Heidi C.E. Welch[1,*]

[1]Signalling Programme, Babraham Institute, Babraham Research Campus, Cambridge CB22 3AT, UK
[2]Beatson Institute for Cancer Research, Switchback Road, Bearsden, Glasgow G61 1BD, UK
[3]Garvan Institute of Medical Research and Kinghorn Cancer Centre, Cancer Research Program, St. Vincent's Clinical School, Faculty of Medicine, University of New South Wales, NSW, 2010 Sydney, Australia
[4]These authors contributed equally to this work
[5]Present address: Research Centre for Animal Genetic Resources of the Mongolia Plateau, Inner Mongolia University, 235 West University Road, 010021 Hohhot, China
*Correspondence: p.timpson@garvan.org.au (P.T.), heidi.welch@babraham.ac.uk (H.C.E.W.)
http://dx.doi.org/10.1016/j.celrep.2014.02.024

SUMMARY

The small G protein family Rac has numerous regulators that integrate extracellular signals into tight spatiotemporal maps of its activity to promote specific cell morphologies and responses. Here, we have generated a mouse strain, Rac-FRET, which ubiquitously expresses the Raichu-Rac biosensor. It enables FRET imaging and quantification of Rac activity in live tissues and primary cells without affecting cell properties and responses. We assessed Rac activity in chemotaxing Rac-FRET neutrophils and found enrichment in leading-edge protrusions and unexpected longitudinal shifts and oscillations during protruding and stalling phases of migration. We monitored Rac activity in normal or disease states of intestinal, liver, mammary, pancreatic, and skin tissue, in response to stimulation or inhibition and upon genetic manipulation of upstream regulators, revealing unexpected insights into Rac signaling during disease development. The Rac-FRET strain is a resource that promises to fundamentally advance our understanding of Rac-dependent responses in primary cells and native environments.

INTRODUCTION

The small G protein family Rac is an essential controller of actin cytoskeletal dynamics and hence cell shape, adhesion, motility, regulated secretion, and phagocytosis, as well as of gene expression and reactive oxygen species (ROS) formation (Heasman and Ridley, 2008; Wennerberg et al., 2005). Rac is active (i.e., able to bind downstream effectors) when guanosine triphosphate (GTP)-bound and inactive when guanosine diphosphate (GDP)-bound. Its activation is catalyzed by at least 20 different DBL- or DOCK-type guanine nucleotide exchange factors (GEFs) (Rossman et al., 2005) and its inhibition by an equally large number of Rac-GTPase-activating proteins (GAPs). Rac downstream signaling specificity and the ensuing Rac-dependent cell responses are largely conferred through the types of GEFs and GAPs that couple Rac to any given upstream signal (Rossman et al., 2005).

Förster resonance energy transfer (FRET) technology is widely used to monitor protein/protein interactions, coupling fluorophore pairs such as cyan fluorescent protein (CFP) and yellow fluorescent protein (YFP) to two proteins of interest. Inter- and intramolecular FRET probes have been used for a decade to visualize Rac activity (Aoki and Matsuda, 2009; Hodgson et al., 2010; Itoh et al., 2002; Kraynov et al., 2000). Intermolecular Rac FRET reporters measure the interaction between separate molecules that must be expressed to comparable levels and subcellular distributions (Kraynov et al., 2000), which can be technically difficult, and they are prone to interfere with endogenous GTPase signaling (Aoki and Matsuda, 2009; Hodgson et al., 2010). The intramolecular "Raichu" (Ras superfamily and interacting protein chimeric unit) Rac-FRET probe contains RAC1 as the signal sensor and Pak-CRIB as the effector, CRIB being the CDC42/Rac interactive binding motif of Pak, a Rac target that binds to GTP-bound, but not GDP-bound, Rac. In Raichu-Rac, RAC1-GTP binding to Pak-CRIB causes FRET from CFP to YFP (Itoh et al., 2002). The probe is anchored into the plasma membrane via a KRAS CAAX motif and hence monitors the balance of endogenous Rac-GEF and Rac-GAP activities at the physiologically relevant subcellular localization of active RAC1 (Itoh et al., 2002).

Rac-FRET biosensors have largely been used in transfection-based experiments in order to correlate the localization of Rac activity with cellular function. Rac is required for cell motility, and use of Rac-FRET probes showed that active Rac localizes to extending cell protrusions during many fundamental processes,

including the leading edge of migrating cells (Itoh et al., 2002; Kraynov et al., 2000; Machacek et al., 2009; Ouyang et al., 2008), forming phagosomal cups during phagocytosis of apoptotic cells (Nakaya et al., 2008), distal poles of daughter cells during cell division (Yoshizaki et al., 2003), or developing neurites during neurogenesis (Aoki et al., 2004). Combining Raichu-Rac expression with downregulation of Vav-family Rac-GEFs showed that phosphatidylinositol 3-kinase-driven GEF membrane targeting localizes Rac activity during neurogenesis (Aoki et al., 2005). Expression of an intermolecular Rac-FRET reporter combined with downregulation of the Rac-GEF TIAM1 showed that TIAM1 association with distinct scaffolding proteins directs localized Rac activity depending on extracellular stimulus (Rajagopal et al., 2010). Similarly, overexpression of a Raichu-Rac-like probe combined with membrane-targeting of TIAM1 or the Rac-GAP chimaerin in Madin-Darby canine kidney (MDCK) cell cysts showed mislocalization of Rac activity to suffice for luminal invasion (Yagi et al., 2012a, 2012b). Finally, use of Raichu-Rac demonstrated apicobasal Rac activity gradients at epithelial cell junctions driven by differential regulation of TIAM1 through β2-syntrophin and Par-3 (Mack et al., 2012).

Raichu-Rac-derived probes are also beginning to be used for monitoring Rac activity in whole tissues. Reporter expression in *Xenopus* and zebrafish embryos showed localized RAC1 activity in migrating cells during organ development (Kardash et al., 2010; Matthews et al., 2008; Xu et al., 2012). A limitation of these studies was that biosensor expression was transient. The first transgenic Rac-FRET biosensor organism was generated recently, a fly that conditionally expresses modified Raichu-Rac in border cells. This revealed Rac activity gradients not only inside cells, but between cell clusters, being highest in cells leading in the direction of migration (Wang et al., 2010). First use of Raichu-Rac-like probes in mammals was recently achieved by transplantation of biosensor-expressing glioblastoma cells into rat brain, thus enabling correlation of Rac activity with the mode of tumor cell migration during invasion (Hirata et al., 2012). Whereas this study was limited by biosensor expression in cultured rather than primary cells, it clearly demonstrated that the mammalian tissue microenvironment controls Rac activity (Hirata et al., 2012).

There is therefore a need for measuring Rac activity in primary mammalian cells and tissues for assessing its regulation by physiologically and functionally relevant organ- or disease-specific environmental cues. Here, we report the development of a Rac-FRET mouse strain, which ubiquitously expresses the original intramolecular Raichu-Rac reporter to allow spatiotemporal quantification of Rac activity in living primary mammalian cells and tissues.

RESULTS

Generation of the Rac-FRET Mouse

We generated a Rac activity reporter mouse strain by introducing the extensively validated intramolecular Raichu-Rac FRET biosensor (Itoh et al., 2002) into the *ROSA26* locus to confer ubiquitous expression from the endogenous promoter. To this end, we first generated Rac-FRET$^{fl/fl}$, a strain in which Raichu-Rac expression was conditionally prevented by a transcriptional stop and crossed this with "deleter," a strain with X-chromosomal *Cre* recombinase, to excise the stop and enable constitutive Raichu-Rac expression before breeding out *Cre* again (Figure S1). Homozygous knockin mice of the resulting Rac-FRET strain were born at expected Mendelian ratio, appeared healthy and fertile, lived normal life-spans, and exhibited no untoward behaviors.

Raichu-Rac Expression Levels in Rac-FRET Mouse Cells and Tissues

Raichu-Rac expression was detected in all tissues tested, at approximately 20–25 ng/mg of tissue, although expression in muscle tissue (heart, stomach, and skeletal muscle) was somewhat lower, at 2–10 ng/mg (Figure 1A). In primary Rac-FRET neutrophils, which express equal amounts of ubiquitous RAC1 and hematopoietic RAC2, expression of the biosensor was 0.6% of endogenous RAC1 and RAC2 (Figure 1B), and in primary E13.5 Rac-FRET mouse embryonic fibroblasts (MEFs), it was 8% of endogenous RAC1 (Figure 1C). Therefore, Raichu-Rac protein levels are low compared to endogenous Rac, as we had aimed for, in order to prevent possible dominant-negative effects. As Raichu-Rac expression did not cause obvious defects and Rac-FRET mice appeared healthy, we continued to characterize properties and responses of primary Rac-FRET MEFs and neutrophils in detail to determine if it affected cell function.

Primary Rac-FRET MEFs Function Normally and Show Highly Localized Rac Activity upon PDGF or Insulin Stimulation

We investigated proliferation, lifespan, and morphology of primary Rac-FRET MEFs. They showed normal proliferation rates, low cell death (2%–4%) in culture, and normal cell morphologies upon serum starvation and platelet-derived growth factor (PDGF) stimulation (Figures S2A–S2C). Pak-CRIB pull-down assays showed that endogenous RAC1 activity was normal in serum-starved and PDGF-stimulated Rac-FRET MEFs, as was the activity of the Rac target p38^{MAPK} (Figures S2D and S2E).

Rac-FRET MEFs were assessed by ratiometric FRET imaging, where increases in YFP/CFP fluorescence ratio induced by FRET reflect increased Rac activity. Treatment with 50 ng/ml PDGF stimulated the formation of lamellipodial protrusions and peripheral membrane ruffles, which showed significantly higher Rac activity (FRET ratio of 1.25) than cell edges without protrusions (FRET ratio of 1.1), and Rac activity remained high throughout lamellipodia formation and ruffling (Figures 2A and 2B; Movie S1). Therefore, Rac activity correlated spatially and temporally with lamellipodia and ruffles, as expected from studies in fibroblast-like cell lines (Itoh et al., 2002). Stimulation with 100 μg/ml insulin, which caused larger lamellipodia but fewer dorsal ruffles, gave similar results (Figure 2C; Movie S2).

Rac-FRET Neutrophils Function Normally and Show High Rac Activity during Spreading and Polarization

We and others have previously shown that Rac and its upstream regulators play crucial roles in ROS formation, adhesion, spreading, and chemotaxis of neutrophils (Deng et al., 2011; Gu et al., 2003; Lawson et al., 2011; Roberts et al., 1999; Welch et al., 2002, 2005), but analysis of Rac activity in these cells has

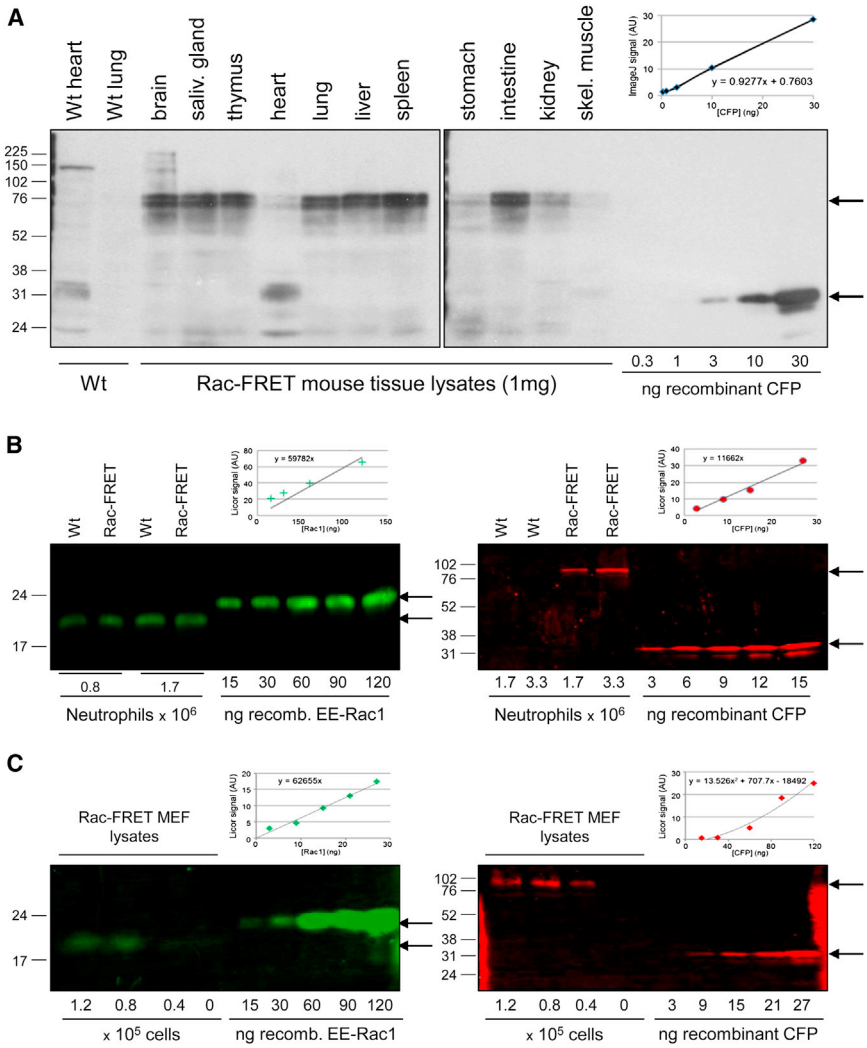

Figure 1. Raichu-Rac Expression Level in Tissues and Primary Cells of the Rac-FRET Mouse Strain

(A) Whole-tissue lysates were prepared from adult Rac-FRET mice and blotted with anti-GFP antibody alongside recombinant CFP standards to reveal the CFP portion of Raichu-Rac. a.u., arbitrary units; WT, wild-type.

(B) Raichu-Rac expression levels in total lysates of the indicated numbers of diisopropyl fluorophosphate-treated Rac-FRET neutrophils were determined by western blotting alongside recombinant RAC1 and CFP standards using anti-RAC1 AB (green) and anti-GFP AB (red) to compare biosensor expression with endogenous RAC1.

(C) Raichu-Rac expression levels in total lysates of the indicated numbers of Rac-FRET MEFs were determined by western blotting alongside recombinant RAC1 and CFP standards with antibodies as in (B).

been hampered by the facts that they are short-lived and cannot easily be transfected. Here, we determined if Rac-dependent neutrophil responses are affected by Raichu-Rac expression. Rac-FRET neutrophils developed normally in the bone marrow (not shown), mounted normal ROS responses to the G protein coupled receptor ligand N-formyl-methionyl-leucyl-phenylalanine (fMLP) and to phorbol myristate acetate (PMA), adhered normally to glass or the integrin ligand poly-Arg-Gly-Asp, spread normally, and underwent normal basal migration and fMLP-stimulated chemotaxis in transwell assays, whereas $Rac2^{-/-}$ cells showed the expected defects (Figures S3A–S3D; Lawson et al., 2011; Roberts et al., 1999). Furthermore, the basal and fMLP-stimulated activities of endogenous RAC1 and RAC2 (by Pak-CRIB pull-down assays) and of the Rac target $p38^{MAPK}$ were normal (Figures S3E–S3G). Therefore, Rac-FRET neutrophil responses were normal by all measures tested.

Rac is required for neutrophil spreading and polarization (Gu et al., 2003; Roberts et al., 1999). We assessed Rac activity during these responses in Rac-FRET neutrophils in the presence or absence of the Rac inhibitor NSC23766. Upon first contact with the coverslip (time 0), Rac activity (normalized FRET ratio) was lower in NSC23766-treated than control cells, but increased initially in both upon adhesion, reaching a maximal value of 1.23 within 8 min in control cells compared to 1.04 in NSC23766-treated cells, and remained high throughout in control cells whereas decreasing to 0.87 with NSC23766 (Figures 3A and 3B). Control cells spread from 90 to 130 μm^2 within 8 min and remained spread, whereas spreading was significantly dampened by NSC23766 (Figure 3C). Rac activity remained high in control cells, correlating with their ability to start polarizing twice as fast as NSC23766-treated cells, to fully polarize and to maintain polarity (Figure 3D). Hence, combined use of NSC23766 and ratiometric FRET imaging showed that Rac activity is required for Rac-FRET neutrophil spreading and polarization, that it increases globally throughout the cell during spreading, and that it remains elevated during polarization.

Rac Activity in Chemotaxing Rac-FRET Neutrophils

Chemotaxing primary murine neutrophils are fast-migrating cells (up to 20 μm/min) that extend transient probing lamellipodial protrusions at their front and sides that typically last for 1 s and longer-lived protrusions (several seconds), mostly at the leading edge, that result in translocation. Here, we assayed Rac activity during chemotaxis of Rac-FRET neutrophils in fMLP gradients (Figure 4A; Movie S3). Ratiometric FRET imaging at 1 s frame intervals showed that high Rac activity correlated spatially with lamellipodial protrusions and low Rac activity with membrane retractions. Temporally, Rac activity was as transient as the protrusions (Figures 4A and 4B). We used polar plots to visualize the localization of Rac activity over time. Comparison with rubber band plots (which depict cell outlines over time) and cell path

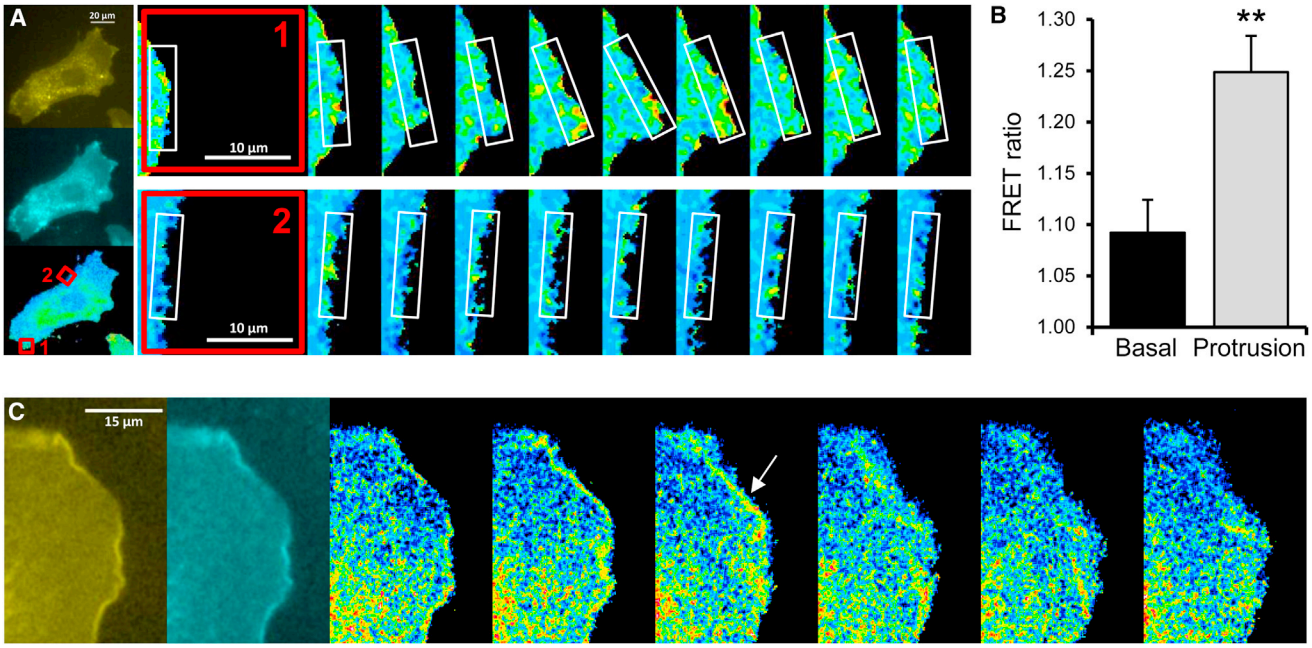

Figure 2. High Rac Activity in Lamellipodial Protrusions and Membrane Ruffles of PDGF-Stimulated Primary Rac-FRET MEFs

(A) Rac activity in PDGF-stimulated (50 ng/ml) Rac-FRET MEFs determined by ratiometric FRET live imaging. Frames were taken every 10 s (left: generation of ratiometric image) and analyzed at protruding (top) and nonprotruding sections (bottom) along the cell edge (magnifications of boxes in the FRET image on the left). Note that, for ratiometric FRET measurements, increase in FRET ratio equals increase in Rac activity.

(B) Quantification of mean Rac activity (FRET ratio ± SEM) in 88 basal and protruding sections along the cell edge of PDGF-stimulated Rac-FRET MEFs as in (A) from 20 cells and three independent experiments. **$p < 0.01$ by paired Student's t test.

(C) Rac activity in insulin-stimulated (100 µg/ml) Rac-FRET MEFs determined by ratiometric FRET imaging. Consecutive frames taken every 10 s, shown from 80 s after addition of insulin (left: YFP/FRET and CFP images used to generate first ratiometric image). Arrow shows Rac activity at membrane ruffles.

plots showed that Rac activity is highest at the leading edge and that bursts of high Rac activity typically last for 3–5 s (Figures 4C, S4A, and S4B). In addition to the leading edge, average polar plots showed bursts of Rac activity at the periphery and trailing edge (Figures S4C and S4D). Detailed analysis of the time dependence of Rac activity and the speed of movement of the cell edge by Pearson's correlation showed a direct correlation (height of peak) between the extent of Rac activity (FRET ratio) and speed of protrusion formation, without any time lag in the order of seconds (alignment of peak with lag = 0 s; Figures 4D and S4E). Therefore, high Rac activity is spatially, temporally, and in magnitude tightly correlated with lamellipodial protrusions at the leading edge of chemotaxing neutrophils.

Oscillations of Rac Activity between the Front and Back of Chemotaxing Rac-FRET Neutrophils

To investigate the bursts of Rac activity at the front versus back of chemotaxing neutrophils further, we line-scanned Rac activity along the central longitudinal axis at 1 s intervals and displayed it as a function of time in kymographs (Figure 4E). This revealed that Rac activity (normalized FRET ratio) is higher at the front of chemotaxing cells than at the back, as expected, but furthermore that the bulk of Rac activity shifts by 1.6 µm toward the posterior of the cell during stalling phases (Figures 4F and S4F). Plotting the location of peak Rac activity on the longitudinal axis against time revealed unexpected oscillations of Rac activity between the front and back of chemotaxing neutrophils, and albeit these oscillations being noisy, they tended toward periodicity. Oscillations of peak Rac activity occurred in all cells analyzed and ranged from 6 to 12 s (mean ± SEM = 8.7 ± 0.4 s), with R^2 values (fit of oscillations to periodicity) ranging from 0.4 to 0.9 (mean = 0.7; Figure 4G). The oscillating peak Rac activity was significantly greater than mean whether localized at the front or the back (Figure S4G). To assess whether the oscillations of Rac activity are characteristic of chemotaxis, we compared control and NSC23766-treated neutrophils. As expected, NSC23766 inhibited chemotaxis (Figure S4Hi), and both mean and peak Rac activity along the central longitudinal axis were lower in NSC23766-treated cells than in control cells (Figure S4Hii). We categorized NSC23766-treated cells that retained some form of movement into those migrating directionally (toward the chemoattractant) and those which had lost directionality (moving nondirectionally, antidirectionally, or without translocation). Oscillations of Rac activity were significantly perturbed in both categories compared to control cells but more so in cells that had lost directionality, as seen by the significant decreases in R^2 value from 0.71 to 0.51 and 0.36, respectively (Figure S4Hiii). These results confirmed that oscillations of Rac activity along the central longitudinal axis of the cell are a hallmark of directional migration in primary mouse neutrophils. Therefore, the use of ratiometric FRET imaging in primary Rac-FRET neutrophils has allowed

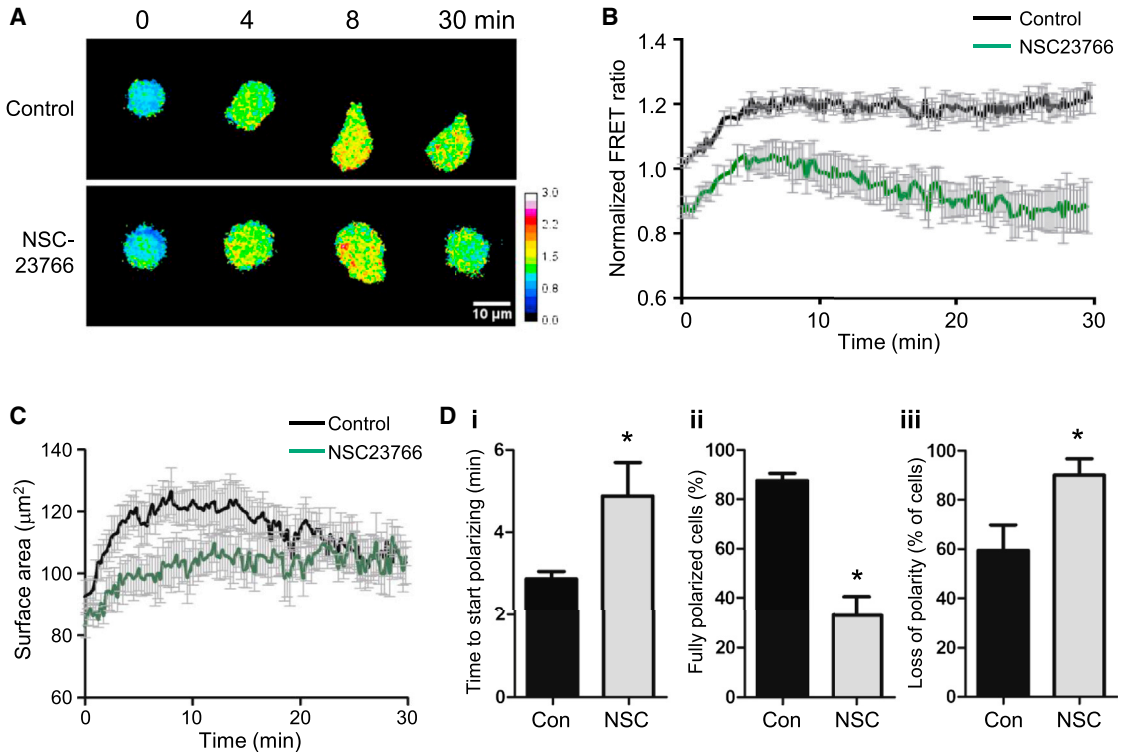

Figure 3. High Rac Activity during Spreading and Polarization of Rac-FRET Neutrophils

(A) Spatiotemporal distribution of Rac activity in Rac-FRET neutrophils during spreading and polarization on glass coverslips was determined by ratiometric FRET live imaging in the presence or absence of 75 μM NSC23766 (without preincubation), starting from the first point of contact of the cells with the coverslip. Representative FRET ratio images are shown.

(B) Quantification of Rac activity (average cellular FRET ratio, normalized to control cells) in 69 control and 59 NSC23766-treated cells as in (A) from six independent experiments ± SEM $p < 0.0001$ by ANOVA.

(C) Surface area of the cells in (B).

(D) Polarization of the cells in (B) was analyzed as: time to start polarizing (i), % of fully polarized cells (as defined by their ability to locomote) (ii), and % of cells reverting to nonpolarized morphology over the 30 min of imaging (iii). *$p < 0.05$ by unpaired Student's t test.

us to reveal unexpected insights into the complexities of Rac signaling during chemotaxis.

Spatiotemporal Regulation of Rac Activity in Mouse Intestinal Crypt Cultures

To examine the spatiotemporal control of Rac activity in a multicellular environment, we generated primary three-dimensional (3D)-intestinal crypt cultures (Myant et al., 2013; Sato et al., 2009) from the Rac-FRET mouse and analyzed them by fluorescence-lifetime imaging microscopy (FLIM)-FRET imaging, where a decrease in CFP fluorescence lifetime due to FRET reflects increased Rac activity. We could readily detect Raichu-Rac expression and image Rac activity in these cultures, which responded to stimulation with 200 nM PMA with a time-dependent increase that peaked after 30 min and subsided after 90 min (Figures 5A and 5B). Rac activity was also spatially regulated. Basal Rac activity was higher in cells at the base of the crypts than in distal cells, and cells at the base of the crypts also responded more strongly to PMA treatment than distal cells (Figures 5A and 5B). This demonstrates reversible and spatial regulation of Rac activity within multicellular mammalian environments, as previously observed in *Drosophila* (Wang et al., 2010).

Effects of Drug Treatment, Genetic Manipulation, and Disease Development on Rac Activity In Vivo

We recently demonstrated that multiphoton microscopy can be used for ex vivo and in vivo FLIM-FRET imaging of murine tumors formed by implanted Raichu-RhoA-expressing pancreatic carcinoma cells (Timpson et al., 2011) and that RHOA activity at the tip of invading tumors correlates with invasion efficiency (McGhee et al., 2011; Timpson et al., 2011). Here, we used similar imaging techniques with the Rac-FRET mouse to examine Rac activity in native host tissue.

Our recent work suggested that increased Rac activity following loss of the tumor suppressor adenomatous polyposis coli (APC) facilitates stem cell hyperproliferation at the base of intestinal crypts and colorectal cancer initiation via enhanced ROS and nuclear factor (NF)-κB production (Myant et al., 2013). To investigate this here, we first evaluated ex vivo multiphoton FLIM-FRET imaging of Rac activity in normal intestinal tissue of the Rac-FRET mouse. Rac activity could be measured within a range of 0–150 μm from the base of crypts toward the villi and was stimulated at the crypt base upon treatment with 200 nM PMA (Figures 5C and 5D; Movie S4). We crossed the Rac-FRET mouse to Vil-Cre-ER^{T2} APC$^{fl/fl}$ mice and induced intestinal

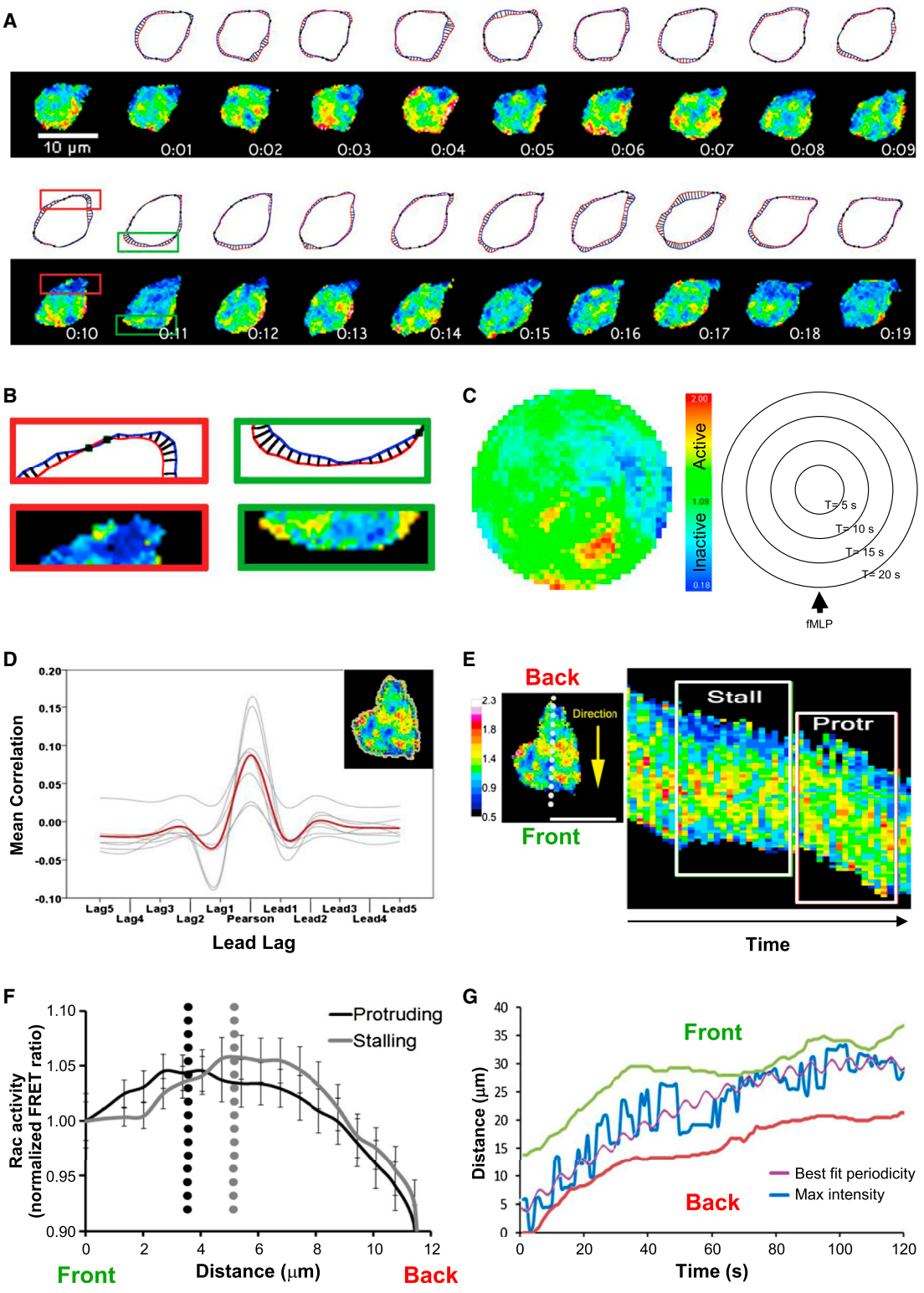

Figure 4. High Rac Activity Correlates with Protrusion Formation at the Leading Edge and Oscillates between the Front and Back of Chemotaxing Rac-FRET Neutrophils

(A) Ratiometric FRET live imaging of a representative Rac-FRET neutrophil chemotaxing toward 3 μM fMLP in an Ibidi chamber; images taken at 1 s intervals over 20 s (chemoattractant source is due south). For comparison of Rac activity with cell protrusions and retractions, cell perimeters at consecutive time points T (blue) and T+1 s (red) were plotted using ImageJ plugin QuimP.

(legend continued on next page)

APC loss by tamoxifen treatment (Myant et al., 2013) to assess the APC dependence of Rac activity in crypts by in vivo FLIM-FRET imaging. APC loss led to increased Rac activity at the base of crypts in Vil-Cre-ER^{T2} APC$^{fl/fl}$ Rac-FRET mice (Figures 5E and 5F), thus demonstrating the utility of the Rac-FRET mouse as a tool for examining the regulation of Rac during disease initiation.

Next, we examined Rac activity in the pancreas in the context of the stromal extracellular matrix (ECM) at depth. Upon stimulation of Rac-FRET mouse pancreas with 200 nM PMA ex vivo, increased Rac activity was observed (Figures 6A and 6B; Movie S5). We crossed the Rac-FRET mouse to the Kras$^{+/G12D}$ Trp53$^{+/R172H}$Pdx1-Cre (KPC) model of pancreatic ductal adenocarcinoma, in which gain-of-function p53^{R172H} drives metastasis on a KRAS^{G12D} background (Morton et al., 2010; Muller et al., 2009). In vivo FLIM-FRET imaging of pancreatic tumors in KPC Rac-FRET mice compared to normal pancreas in Rac-FRET mice revealed that Rac activity was significantly upregulated in tumors (Figures 6C and 6D). Such deregulated Rac activity may partially explain the disruption of cell-cell and cell-matrix adhesion and tumor dissociation, which characterize this invasive and highly metastatic model (Morton et al., 2010; Muller et al., 2009, 2013).

We also crossed the Rac-FRET mouse to the locally invasive Polyoma-middle T (PyMT) breast cancer model. Rac activity could readily be detected in isolated primary mammary tumors of PyMT Rac-FRET mice and inhibited by NSC23766 treatment (Figures 7A and 7B; Movie S6). In vivo FLIM-FRET imaging of exposed tumor tissue of PyMT Rac-FRET mice injected with NSC23766 showed that Rac was inactivated within 60 min of NSC23766 administration and began to revert to control level after 90 min (Figures 7C and 7D). This highlights the utility of the Rac-FRET mouse for monitoring drug target activity and clearance rates, which could be applied to guide the scheduling and dosing of therapeutic intervention.

Finally, we have recently shown that the Rac-GEF PREX1 is deregulated in melanoma and drives Rac-dependent invasion (Li et al., 2011; Lindsay et al., 2011). To assess whether the Rac-FRET mouse is useful for examining Rac activity in the skin, while at the same time trialling tissue-specific expression, we crossed Rac-FRET$^{fl/fl}$ to K14-Cre mice to induce selective Raichu-Rac expression in keratinocytes. Rac activity could readily be detected by FLIM-FRET imaging of E15.5 K14-Cre Rac-FRET$^{fl/fl}$ embryonic skin explants and stimulated by PMA treatment (Figure S5; Movie S7). Combined with PREX1 deficiency, this may be useful for examining PREX1 in melanoma metastasis. Collectively, the assessment of Rac activity within these and other organs, such as the liver (Figure S6; Movie S8), emphasizes the general utility and scope of the Rac-FRET mouse as a tool for monitoring the intricate mechanisms of regulation of Rac signaling in a myriad of physiological processes and disease states.

DISCUSSION

Here, we report the development of a Rac-FRET mouse that ubiquitously expresses Raichu-Rac. We examined Rac activity in primary MEFs, neutrophils, and intestinal crypts, as well as in intact tissues (intestine, liver, mammary, pancreas, and skin), in response to genetic or drug intervention. This revealed unexpected insights into Rac signaling during neutrophil chemotaxis, tissue homeostasis, disease initiation, and disease progression.

We chose the Raichu-Rac reporter over other Rac-FRET biosensors as the probe most likely to provide best signal-to-noise ratio without affecting cell survival. A similar Raichu-Rac probe with a RAC1 instead of a KRAS membrane-targeting cassette gives higher background (Yoshizaki et al., 2003); another probe that uses CRIB between CFP and YFP, measuring FRET inhibition upon binding of endogenous Rac (Graham et al., 2001), is neither as sensitive as Raichu-Rac nor specific for Rac, as it also binds CDC42-GTP; and finally a Raichu-like probe in which YFP is replaced with more sensitive YPet (Ouyang et al., 2008) suggested nonnegligible cytotoxicity in our hands. Recently, progress in the development of Raichu sensors involving longer linkers in the reporter molecule has been made, reducing basal FRET further and thus increasing signal-to-noise (Komatsu et al., 2011). A next step in reporter mouse development could be the use of such an improved construct.

The *ROSA26* locus was chosen for its ubiquitous expression, and the endogenous *ROSA26* promoter, rather than stronger

(B) Enlargement of boxed sections shown in (A). The green-framed box shows a protrusion at the leading edge of the cell, the red box a retraction at the trailing edge.

(C) Polar plot of Rac activity (FRET ratio) around the perimeter of the cell shown in (A) over time; perimeters depicted as perfect circles, 1 circle/1 s time frame, starting in the center (1 s) and growing eccentrically outward over time.

(D) Pearson's correlation between Rac activity (FRET ratio) at nodes around the cell perimeter and 0.4 μm from the cell edge (schematic example shown in insert) and cell edge velocity. FRET intensities were evaluated against edge speeds between T−5 s and T+5 s to test for time dependence between Rac activity and membrane protrusion/retraction speed. Red line shows average correlation from seven independent experiments with a total of 133 cells chemotaxing toward 3 μM fMLP over 100–120 s with images acquired every 1 s; gray traces show means of individual experiments.

(E) Rac-FRET neutrophils chemotaxing toward 3 μM fMLP in an Ibidi chamber were live imaged at 1 s intervals, line scans performed through the central longitudinal axis, and Rac activity (FRET ratio) over time plotted as kymographs. Profiling of steep (protruding) versus flat (stalling) sections of the kymograph was achieved by averaging line scans for each segment (as detailed in Supplemental Experimental Procedures). Average speed was 15 μm/min during protruding and 4.2 μm/min during stalling phases of migration.

(F) Average Rac activity (FRET ratio) in central longitudinal line scans of 25 cells from five independent experiments. Gray and black dotted lines show the distance of the peak Rac activity from the front edge during protruding and stalling phases of migration. The extent of the retrograde shift was 1.6 μm during stalling phases (mean of 25 cells; five experiments; paired t test $p = 0.02$).

(G) Rac activity oscillates between the front and the back of chemotaxing neutrophils. Maximum Rac activity (blue) along the central longitudinal axis of a representative chemotaxing neutrophil was plotted for each 1 s time frame in order to allow an assessment of the spatial localization of the point of highest Rac activity over time, and best fit periodicity curves (purple) were applied to evaluate the oscillations. The position of the front of the cell at each time point is traced in green, that of the back in red. Data shown are from one cell representative of 19 cells analyzed.

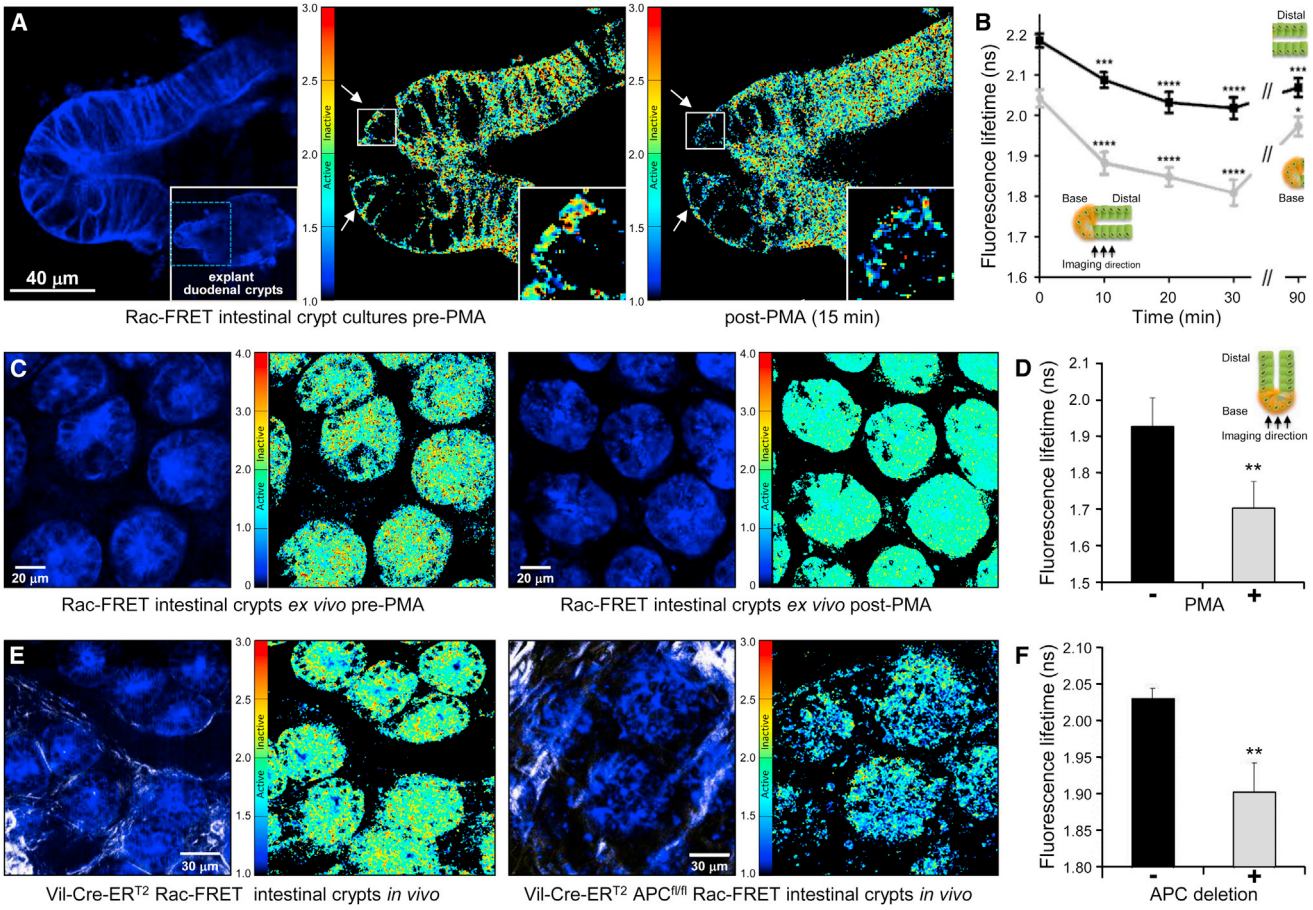

Figure 5. Spatiotemporal Distribution of Rac Activity in Intestinal Tissue

(A) PMA stimulation of Rac activity at the base is stronger than in distal cells of Rac-FRET duodenal crypt cultures. Representative fluorescence image of an intestinal crypt culture (left) with Raichu-Rac (blue) and corresponding FLIM-FRET fluorescence lifetime maps of Rac activity before (middle) or after (right) 200 nM PMA treatment. In the FLIM-FRET images, arrows highlight the crypt base and insets show enlarged boxed sections. Note that, for FLIM-FRET measurements, decrease in fluorescence lifetime equals increase in Rac activity.

(B) Quantification of Rac activity in intestinal crypt cultures as in (A) upon stimulation with 200 nM PMA for 0–90 min. Mean fluorescence lifetime ± SEM of 21–31 cells at varying positions in the base (black) or the distal section of the crypt (gray), as indicated by the schematics, for each time point and location. *$p < 0.05$, ***$p < 0.001$, and ****$p < 0.0001$ by unpaired Student's t test between indicated time and 0-time control.

(C) Rac activity at the base of Rac-FRET intestinal crypts is stimulated by PMA ex vivo. Representative FLIM-FRET images before (left) and after (right) stimulation of freshly isolated intestinal crypt tissue with 200 nM PMA for 15 min. For each pair of images, the left-hand panel shows a representative fluorescence image of intestinal crypts expressing Raichu-Rac (blue), the right-hand one a corresponding fluorescence lifetime map.

(D) Quantification of Rac activity (fluorescence lifetime; mean ± SEM) at the base of 20 intestinal Rac-FRET mouse intestinal crypts before and after PMA stimulation ex vivo as in (C).

(E) Rac activity at the base of intestinal crypts is increased upon tissue-specific APC loss in vivo. Representative FLIM-FRET images at the base of intestinal crypts of live Vil-Cre-ER^{T2} Rac-FRET control mice (left) and Vil-Cre-ER^{T2} APC$^{fl/fl}$ Rac-FRET mice with intestinal tissue-specific APC deletion (right). For each pair of images, the left-hand panel shows a representative fluorescence image of intestinal crypts expressing Raichu-Rac (blue) and the second harmonic generation (SHG) signal from host ECM components (white), the right-hand one a corresponding fluorescence lifetime map.

(F) Quantification of Rac activity (fluorescence lifetime; mean ± SEM) from 206 cells at the base of intestinal crypts in control mice and 197 cells in APC-deleted mice as in (E); three independent regions each. **$p < 0.05$ by unpaired Student's t test.

exogenous promoters, to deliberately aim for low expression levels to prevent conceivable dominant-negative effects. We introduced Raichu-Rac with a floxed stop cassette for either ubiquitous or conditional expression, depending on the choice of *Cre*-recombinase strain. The Rac-FRET mouse expresses Raichu-Rac constitutively and ubiquitously. Our assessment of MEFs and neutrophils showed that we gauged expression level well, high enough for detection, but not affecting cell properties or responses. However, particularly in neutrophils, signal strength is limiting, so development of a strain with stronger inducible expression may be useful. Crossing of Rac-FRET$^{fl/fl}$ to K14-Cre mice demonstrated that the conditional Rac-FRET$^{fl/fl}$ strain is useful for tissue-specific expression of Raichu-Rac. Such targeted expression of the reporter will allow the assessment of Rac activity in specific cell types within heterogeneous tissues. For example, Lgr5-Cre mice (Barker et al.,

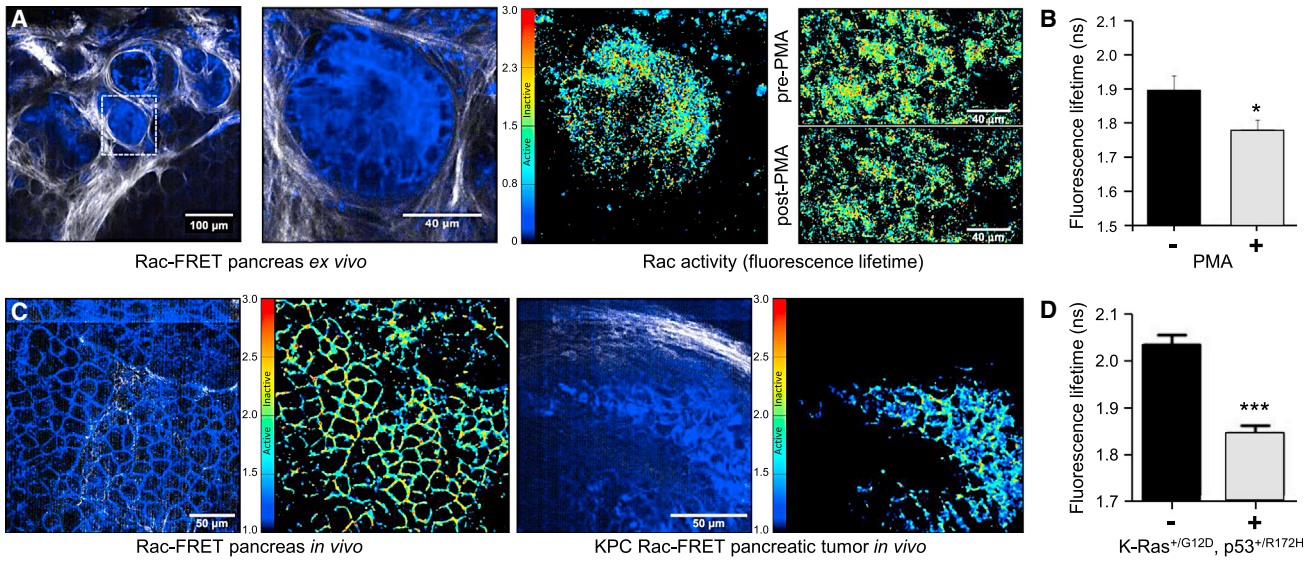

Figure 6. High Rac Activity in Pancreatic Tumors

(A) Rac activity is stimulated by PMA in Rac-FRET mouse pancreas ex vivo. From the left, panels show a fluorescence image of freshly isolated pancreatic tissue, an enlargement of the region analyzed, with Raichu-Rac expression in blue and SHG signal from host ECM in white, a corresponding Rac activity (fluorescence lifetime) map, and images of Rac activity before (top) and after (bottom) treatment with 200 nM PMA for 15 min.

(B) Quantification of pancreatic Rac activity (fluorescence lifetime; mean ± SE) as in (A) from 30 cells in three regions before and after stimulation with 200 nM PMA for 15 min. *$p < 0.05$ by unpaired Student's t test. ns, not significant.

(C) Increased Rac activity in pancreatic tumors in vivo. Representative FLIM-FRET images comparing normal pancreas in live Rac-FRET mice and pancreatic tumors in live KPC Rac-FRET mice. For each pair of images, the left-hand panel shows a representative fluorescence image of Raichu-Rac (blue) and SHG signal from host ECM (white), the right-hand one a corresponding FLIM-FRET fluorescence lifetime map.

(D) Quantification of Rac activity in Rac-FRET and KPC Rac-FRET pancreas in vivo as in (C). Mean fluorescence lifetime ± SEM of 222 Rac-FRET and 461 KPC Rac-FRET cells from three to four regions/mouse, three mice/genotype. ***$p < 0.001$ by unpaired Student's t test.

2007) could be used in the future to express Raichu-Rac specifically in stem cells of the small intestine to investigate further the increased Rac activity we observed upon deletion of the tumor suppressor APC. Alternatively, the Rac-FRET mouse could be crossed to a strain expressing a red fluorescent protein specifically in a cell type of interest, for in vivo colabeling and comparing Rac activity between specific cell types within complex tissues. We also crossed Rac-FRET$^{fl/fl}$ with Cre-ER^{T2} mice for drug-inducible expression (Feil et al., 1996). Cre-ER$^{+/T2}$ Rac-FRET$^{+/fl}$ neutrophils expressed similar levels of Raichu-Rac upon tamoxifen treatment than Rac-FRET neutrophils and showed normal cell responses. Thus, inducible Raichu-Rac expression is another useful feature of the Rac-FRET$^{fl/fl}$ strain.

Crossing the Rac-FRET mouse to various models of disease has demonstrated its utility for assessing the effects of mutations that recapitulate human disease etiology on Rac activity in a time- and tissue-specific manner, even in organs and tissues that contain complex mixtures of cell types, without affecting tissue homeostasis. For example, in colorectal cancer, APC loss often leads to hyperproliferation of intestinal stem cells, and RAC1 is a critical mediator of this process through its roles in ROS production and NF-κB signaling (Myant et al., 2013). Therefore, it is unsurprising that we found the Rac pathway to be active upon APC loss. We suspect that, in normal intestinal tissue, the basal and PMA-stimulated Rac activities were also higher in cells at the base of crypts than in distal cells because the highly proliferative intestinal stem cells are located there. As another example for possible future applications, crossing the Rac-FRET mouse with Tyr-Cre strain for melanoblast-specific expression (Delmas et al., 2003), with Prex1$^{-/-}$ mice or with murine models of melanoma, could provide insights into the cell-type- and stage-specific roles of Rac deregulation during melanoma progression (Li et al., 2011; Lindsay et al., 2011).

Ratiometric FRET microscopy was useful for measurement of Rac activity in isolated primary Rac-FRET neutrophils and MEFs. Similarly, ratiometric FRET was chosen in Rac-FRET reporter-expressing zebrafish embryos, because of their optical transparency (Kardash et al., 2010; Xu et al., 2012). In thick tissue or organ sections, multiphoton FLIM-FRET imaging allowed us to monitor tissues at depth and with high resolution, both ex vivo and in vivo, in the context of the host tissue and environmental cues. Considering recent advances in imaging and image analysis, which allow millisecond resolution of spatiotemporal dynamics (Hinde et al., 2013), it should be possible to adapt imaging systems to analyze Rac activity alongside Rac-dependent cell responses in any type of tissue.

Use of the Rac-FRET mouse allowed us to observe the exquisite spatiotemporal regulation of Rac activity in primary neutrophils, which are very different from even their closest model cell lines, e.g., in their formation of more-transient and probing lamellipodial protrusions during chemotaxis, which we show here to be accompanied by equally transient and locally restricted bursts of Rac activity. During the initial phase of neutrophil spreading, we observed some increase in Rac

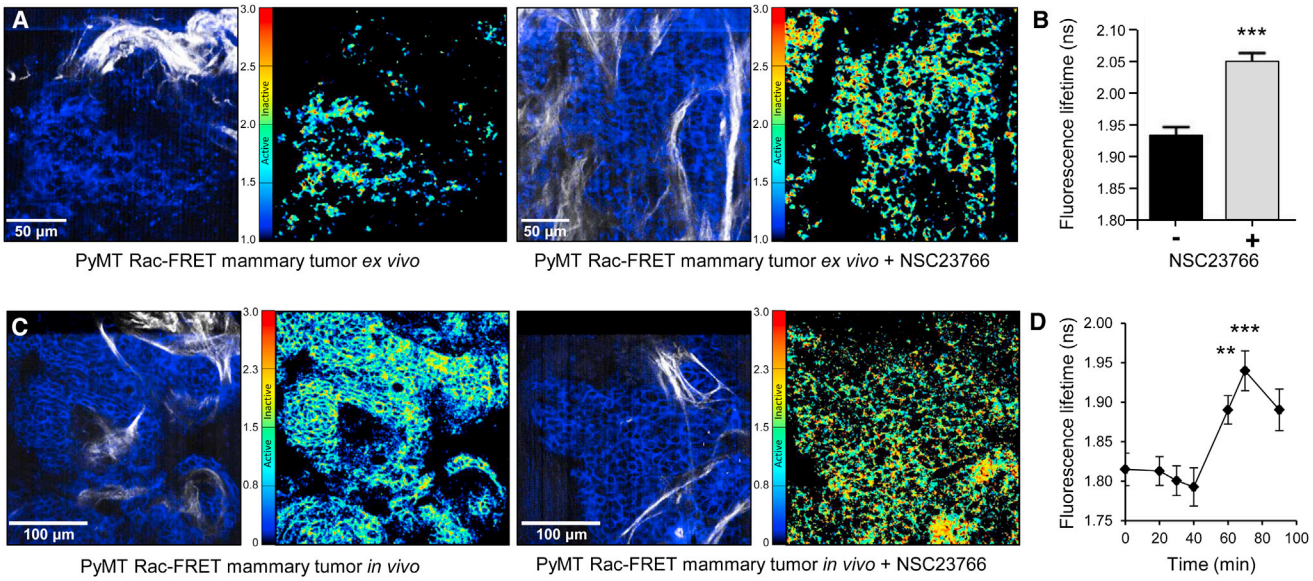

Figure 7. Rac Activity in Mammary Tumors Is Inhibited by NSC23766

(A) Rac activity in PyMT Rac-FRET mouse mammary tumors is inhibited by NSC23766 ex vivo. Representative FLIM-FRET images of freshly isolated mammary tumors of PyMT Rac-FRET mice without (left) or with (right) treatment with 50 μM NSC23766 for 60 min ex vivo. For each pair of images, the left-hand panel shows a representative fluorescence image of tissue expressing Raichu-Rac (blue) and SHG signal from host ECM (white), the right-hand one a corresponding Rac activity (fluorescence lifetime) map.

(B) Quantification of Rac activity in PyMT mammary tumors as in (A). Mean fluorescence lifetime ± SEM of 144 control cells and 74 NSC23766-treated cells from two to three different regions/group. ***$p < 0.001$ by unpaired Student's t test.

(C) Rac activity in mammary tumors is inhibited by treatment with NSC23766 in vivo. Representative FLIM-FRET images of Rac activity in mammary tumors of live PyMT Rac-FRET mice before (left) and 60 min after (right) intraperitoneal (i.p.) injection of NSC23766 (4 mg/kg). Order of images as in (A).

(D) Quantification of Rac activity (fluorescence lifetime; mean ± SEM) in 210 cells within mammary tumors of PyMT Rac-FRET mice in vivo 0–90 min after i.p. injection of NSC23766. **$p < 0.01$ and ***$p < 0.001$ by unpaired Student's t test.

activity, even in NSC23766-treated cells (though lower than in controls). This could simply be due to incomplete inhibition, but it is also possible that NSC23766-insensitive Rac-GEFs might contribute to this phase. Rac-GEFs from the Vav family, for example, are nonresponsive to NSC23766 (Gao et al., 2004) and known to be required for neutrophil spreading (Lawson et al., 2011). This possibility could be investigated in the future by analysis of Rac-FRET neutrophils with added Rac-GEF deficiencies. During neutrophil chemotaxis, we observed unexpected behaviors of Rac activity in addition to the expected accumulation at the leading edge, including a retrograde shift during stalling phases and a yo-yoing between the front and back of the cell. It is unsurprising that these phenomena have not been observed previously, as only a combination of FRET technology and the use of primary cells affords sufficient spatiotemporal resolution. Wider and slower waves of Rac activity had previously been observed in HL60 cells (Weiner et al., 2007), and it seems possible that the oscillations in primary cells are mechanistically related. It will be interesting to determine if specific upstream regulators mediate these oscillations and if these Rac-GEFs are required for the fast migration mode of neutrophils.

Different types of small G proteins of the Rho family are activated dependently of each other. Combined use of Rac, CDC42, or RHOA activity probes and high-resolution imaging of single-membrane protrusions showed that RhoA is activated at the tip of forming cell protrusions whereas Rac and CDC42 activity patterns are wider (Machacek et al., 2009). Furthermore, transplantation of glioblastoma cells expressing Rac, CDC42, or RHOA reporters into rat brain suggested that the balance of Rac, CDC42, and RHOA activities dictates modes of cancer cell invasion (Hirata et al., 2012). Transgenic biosensor mice for a number of different types of small G proteins are currently being generated (Goto et al., 2013), although not as conditional alleles and at much higher expression levels. Such GTPase reporter mice will facilitate future comparisons between different small G proteins tremendously, and different strains will doubtless prove appropriate for different applications.

In conclusion, the Rac-FRET mouse strain has enabled us to monitor the intricate and dynamic regulation of the small G protein Rac, an essential controller of distinct biological responses depending on timing, location, and signaling context. Future use of the Rac-FRET mouse as a tool, alone or in combination with deficiencies in Rac-GEFs, Rac-GAPs, or other upstream regulators, should fundamentally advance our insight into the signaling networks that drive Rac-dependent cell responses and enable us to expand our knowledge of Rac signaling in primary cells and complex multicellular physiological and disease states.

EXPERIMENTAL PROCEDURES

Detailed protocols can be found in Supplemental Experimental Procedures.

Generation of the Rac-FRET Reporter Mouse Strain

Modified Raichu-1011X plasmid (Itoh et al., 2002) was introduced into stop-eGFP-ROSA26TV (Addgene 11739) to generate the Rac-FRET targeting vector. Upon germline transmission, Rac-FRET$^{fl/fl}$ strain was crossed with deleter to induce ubiquitous expression of Raichu-Rac. The resulting homozygous Rac-FRET$^{Ki/Ki}$ knockin mouse strain was called Rac-FRET for brevity. Raichu-Rac expression in cells and tissues of the Rac-FRET mouse was determined by western blotting.

Rac-FRET MEF and Neutrophil Isolation and Responses

Primary E13.5 MEFs were isolated upon timed mating of Rac-FRET$^{Ki/fl}$ mice and cultured for up to 15 days. Proliferation assays were done by cell counting, cell cycle assays by propidium iodide staining, and morphology assays by image analysis of tetramethylrhodamine isothiocyanate-phalloidin-stained cells. Primary neutrophils were freshly isolated from bone marrow for each experiment. Adhesion and spreading were assayed on glass or integrin-ligand surfaces, ROS formation by luminol assay, and chemotaxis by transwell assays using 3 μm pore filters (Lawson et al., 2011; Welch et al., 2005) or Ibidi chamber assays using Ibidi sticky slide IV$^{0.4}$. Endogenous Rac activity was determined in Rac-FRET MEF and neutrophil lysates by Pak-CRIB pull-down and p38^{MAPK} phosphorylation by western blotting.

Tissues and Mouse Strains for Analysis of Rac Activity in Live Tissues and Organs

Intestinal crypt cultures (Sato et al., 2009) and skin explants (Mort et al., 2010) were prepared as described. Vil-Cre-ER^{T2} APC$^{fl/fl}$ Rac-FRET mice for imaging of Rac activity in intestinal crypts following APC loss, KPC Rac-FRET mice for imaging of Rac activity in pancreatic tumors, PyMT Rac-FRET mice for imaging of Rac activity in mammary tumors, and K14-Cre Rac-FRET$^{fl/fl}$ mice for tissue-specific expression of Raichu-Rac and imaging of Rac activity in embryonic skin were generated as detailed in Supplemental Experimental Procedures.

Imaging

Rac activity was assessed in Rac-FRET MEFs and neutrophils by ratiometric FRET imaging using an Olympus Cell^R imaging system. Pairs of images were acquired sequentially every 15 s for spreading neutrophils and every 10 s for MEFs. For chemotaxing neutrophils, both channels were acquired simultaneously at 1 frame/s and cells tracked using ImageJ plugin QuimP11. Pearson's correlation was used to analyze the time dependence between Rac activity and speed of cell edge movement and polar plots (Ferguson et al., 2007) for the spatiotemporal representation of Rac activity at the cell perimeter. In addition, line scans of Rac activity were performed along the central longitudinal axis.

Imaging of Rac activity in various intact tissues and organs was done using multiphoton FLIM-FRET imaging. Crypt cultures were imaged at depths of 0–100 μm and freshly isolated ex vivo crypts (Myant et al., 2013) at 0–150 μm. For in vivo imaging of intestinal, pancreas, or mammary tissue, mice were terminally anesthetized. Multiphoton FLIM-FRET imaging was carried out on a Nikon Eclipse TE2000-U inverted microscope with an Olympus long working distance 20 × 0.95 numerical aperture water immersion lens using a scan head specifically designed for multiphoton excitation. Data were analyzed using the time-correlated single-photon counting fluorescence lifetime analysis functionality of ImSpectorPro (LaVison Biotec).

SUPPLEMENTAL INFORMATION

Supplemental Information includes Supplemental Experimental Procedures, six figures, and eight movies and can be found with this article online at http://dx.doi.org/10.1016/j.celrep.2014.02.024.

ACKNOWLEDGMENTS

We are extremely grateful to Miki Matsuda for allowing us to generate the Rac-FRET mouse with the Raichu-Rac construct and for constructively discussing the choice of construct with us at the beginning of the project. We acknowledge the great skill of the people from the Babraham and Beatson animal facilities and the passionate care they take in looking after our mice. We also thank James Conway for critical reading of the manuscript. The project was funded by BBSRC core funding, BBSRC grant BB/I02154X/1, CRUK core funding, and NHMRC and ARC funding. Work in the O.J.S. lab was funded through European Union PRIMES project grant FP7-HEALTH-2011-278568.

Received: November 20, 2013
Revised: February 5, 2014
Accepted: February 15, 2014
Published: March 13, 2014

REFERENCES

Aoki, K., and Matsuda, M. (2009). Visualization of small GTPase activity with fluorescence resonance energy transfer-based biosensors. Nat. Protoc. *4*, 1623–1631.

Aoki, K., Nakamura, T., and Matsuda, M. (2004). Spatio-temporal regulation of Rac1 and Cdc42 activity during nerve growth factor-induced neurite outgrowth in PC12 cells. J. Biol. Chem. *279*, 713–719.

Aoki, K., Nakamura, T., Fujikawa, K., and Matsuda, M. (2005). Local phosphatidylinositol 3,4,5-trisphosphate accumulation recruits Vav2 and Vav3 to activate Rac1/Cdc42 and initiate neurite outgrowth in nerve growth factor-stimulated PC12 cells. Mol. Biol. Cell *16*, 2207–2217.

Barker, N., van Es, J.H., Kuipers, J., Kujala, P., van den Born, M., Cozijnsen, M., Haegebarth, A., Korving, J., Begthel, H., Peters, P.J., and Clevers, H. (2007). Identification of stem cells in small intestine and colon by marker gene Lgr5. Nature *449*, 1003–1007.

Delmas, V., Martinozzi, S., Bourgeois, Y., Holzenberger, M., and Larue, L. (2003). Cre-mediated recombination in the skin melanocyte lineage. Genesis *36*, 73–80.

Deng, Q., Yoo, S.K., Cavnar, P.J., Green, J.M., and Huttenlocher, A. (2011). Dual roles for Rac2 in neutrophil motility and active retention in zebrafish hematopoietic tissue. Dev. Cell *21*, 735–745.

Feil, R., Brocard, J., Mascrez, B., LeMeur, M., Metzger, D., and Chambon, P. (1996). Ligand-activated site-specific recombination in mice. Proc. Natl. Acad. Sci. USA *93*, 10887–10890.

Ferguson, G.J., Milne, L., Kulkarni, S., Sasaki, T., Walker, S., Andrews, S., Crabbe, T., Finan, P., Jones, G., Jackson, S., et al. (2007). PI(3)Kgamma has an important context-dependent role in neutrophil chemokinesis. Nat. Cell Biol. *9*, 86–91.

Gao, Y., Dickerson, J.B., Guo, F., Zheng, J., and Zheng, Y. (2004). Rational design and characterization of a Rac GTPase-specific small molecule inhibitor. Proc. Natl. Acad. Sci. USA *101*, 7618–7623.

Goto, A., Sumiyama, K., Kamioka, Y., Nakasyo, E., Ito, K., Iwasaki, M., Enomoto, H., and Matsuda, M. (2013). GDNF and endothelin 3 regulate migration of enteric neural crest-derived cells via protein kinase A and Rac1. J. Neurosci. *33*, 4901–4912.

Graham, D.L., Lowe, P.N., and Chalk, P.A. (2001). A method to measure the interaction of Rac/Cdc42 with their binding partners using fluorescence resonance energy transfer between mutants of green fluorescent protein. Anal. Biochem. *296*, 208–217.

Gu, Y., Filippi, M.D., Cancelas, J.A., Siefring, J.E., Williams, E.P., Jasti, A.C., Harris, C.E., Lee, A.W., Prabhakar, R., Atkinson, S.J., et al. (2003). Hematopoietic cell regulation by Rac1 and Rac2 guanosine triphosphatases. Science *302*, 445–449.

Heasman, S.J., and Ridley, A.J. (2008). Mammalian Rho GTPases: new insights into their functions from in vivo studies. Nat. Rev. Mol. Cell Biol. *9*, 690–701.

Hinde, E., Digman, M.A., Hahn, K.M., and Gratton, E. (2013). Millisecond spatiotemporal dynamics of FRET biosensors by the pair correlation function and the phasor approach to FLIM. Proc. Natl. Acad. Sci. USA *110*, 135–140.

Hirata, E., Yukinaga, H., Kamioka, Y., Arakawa, Y., Miyamoto, S., Okada, T., Sahai, E., and Matsuda, M. (2012). In vivo fluorescence resonance energy

transfer imaging reveals differential activation of Rho-family GTPases in glioblastoma cell invasion. J. Cell Sci. *125*, 858–868.

Hodgson, L., Shen, F., and Hahn, K. (2010). Biosensors for characterizing the dynamics of rho family GTPases in living cells. In Current Protocols in Cell Biology, Chapter 14, J.S. Bonifacino, M. Dasso, J.B. Harford, J. Lippincott-Schwartz, and K.M. Yamada, eds. (New York: John Wiley & Sons), pp. 11–26.

Itoh, R.E., Kurokawa, K., Ohba, Y., Yoshizaki, H., Mochizuki, N., and Matsuda, M. (2002). Activation of rac and cdc42 video imaged by fluorescent resonance energy transfer-based single-molecule probes in the membrane of living cells. Mol. Cell. Biol. *22*, 6582–6591.

Kardash, E., Reichman-Fried, M., Maître, J.L., Boldajipour, B., Papusheva, E., Messerschmidt, E.M., Heisenberg, C.P., and Raz, E. (2010). A role for Rho GTPases and cell-cell adhesion in single-cell motility in vivo. Nat. Cell Biol. *12*, 47–53, 1–11.

Komatsu, N., Aoki, K., Yamada, M., Yukinaga, H., Fujita, Y., Kamioka, Y., and Matsuda, M. (2011). Development of an optimized backbone of FRET biosensors for kinases and GTPases. Mol. Biol. Cell *22*, 4647–4656.

Kraynov, V.S., Chamberlain, C., Bokoch, G.M., Schwartz, M.A., Slabaugh, S., and Hahn, K.M. (2000). Localized Rac activation dynamics visualized in living cells. Science *290*, 333–337.

Lawson, C.D., Donald, S., Anderson, K.E., Patton, D.T., and Welch, H.C. (2011). P-Rex1 and Vav1 cooperate in the regulation of formyl-methionyl-leucyl-phenylalanine-dependent neutrophil responses. J. Immunol. *186*, 1467–1476.

Li, A., Ma, Y., Yu, X., Mort, R.L., Lindsay, C.R., Stevenson, D., Strathdee, D., Insall, R.H., Chernoff, J., Snapper, S.B., et al. (2011). Rac1 drives melanoblast organization during mouse development by orchestrating pseudopod- driven motility and cell-cycle progression. Dev. Cell *21*, 722–734.

Lindsay, C.R., Lawn, S., Campbell, A.D., Faller, W.J., Rambow, F., Mort, R.L., Timpson, P., Li, A., Cammareri, P., Ridgway, R.A., et al. (2011). P-Rex1 is required for efficient melanoblast migration and melanoma metastasis. Nat. Commun. *2*, 555.

Machacek, M., Hodgson, L., Welch, C., Elliott, H., Pertz, O., Nalbant, P., Abell, A., Johnson, G.L., Hahn, K.M., and Danuser, G. (2009). Coordination of Rho GTPase activities during cell protrusion. Nature *461*, 99–103.

Mack, N.A., Porter, A.P., Whalley, H.J., Schwarz, J.P., Jones, R.C., Khaja, A.S., Bjartell, A., Anderson, K.I., and Malliri, A. (2012). β2-syntrophin and Par-3 promote an apicobasal Rac activity gradient at cell-cell junctions by differentially regulating Tiam1 activity. Nat. Cell Biol. *14*, 1169–1180.

Matthews, H.K., Marchant, L., Carmona-Fontaine, C., Kuriyama, S., Larraín, J., Holt, M.R., Parsons, M., and Mayor, R. (2008). Directional migration of neural crest cells in vivo is regulated by Syndecan-4/Rac1 and non-canonical Wnt signaling/RhoA. Development *135*, 1771–1780.

McGhee, E.J., Morton, J.P., Von Kriegsheim, A., Schwarz, J.P., Karim, S.A., Carragher, N.O., Sansom, O.J., Anderson, K.I., and Timpson, P. (2011). FLIM-FRET imaging in vivo reveals 3D-environment spatially regulates RhoGTPase activity during cancer cell invasion. Small GTPases *2*, 239–244.

Mort, R.L., Hay, L., and Jackson, I.J. (2010). Ex vivo live imaging of melanoblast migration in embryonic mouse skin. Pigment Cell Melanoma Res. *23*, 299–301.

Morton, J.P., Timpson, P., Karim, S.A., Ridgway, R.A., Athineos, D., Doyle, B., Jamieson, N.B., Oien, K.A., Lowy, A.M., Brunton, V.G., et al. (2010). Mutant p53 drives metastasis and overcomes growth arrest/senescence in pancreatic cancer. Proc. Natl. Acad. Sci. USA *107*, 246–251.

Muller, P.A., Caswell, P.T., Doyle, B., Iwanicki, M.P., Tan, E.H., Karim, S., Lukashchuk, N., Gillespie, D.A., Ludwig, R.L., Gosselin, P., et al. (2009). Mutant p53 drives invasion by promoting integrin recycling. Cell *139*, 1327–1341.

Muller, P.A., Trinidad, A.G., Timpson, P., Morton, J.P., Zanivan, S., van den Berghe, P.V., Nixon, C., Karim, S.A., Caswell, P.T., Noll, J.E., et al. (2013). Mutant p53 enhances MET trafficking and signalling to drive cell scattering and invasion. Oncogene *32*, 1252–1265.

Myant, K.B., Cammareri, P., McGhee, E.J., Ridgway, R.A., Huels, D.J., Cordero, J.B., Schwitalla, S., Kalna, G., Ogg, E.L., Athineos, D., et al. (2013). ROS production and NF-κB activation triggered by RAC1 facilitate WNT-driven intestinal stem cell proliferation and colorectal cancer initiation. Cell Stem Cell *12*, 761–773.

Nakaya, M., Kitano, M., Matsuda, M., and Nagata, S. (2008). Spatiotemporal activation of Rac1 for engulfment of apoptotic cells. Proc. Natl. Acad. Sci. USA *105*, 9198–9203.

Ouyang, M., Sun, J., Chien, S., and Wang, Y. (2008). Determination of hierarchical relationship of Src and Rac at subcellular locations with FRET biosensors. Proc. Natl. Acad. Sci. USA *105*, 14353–14358.

Rajagopal, S., Ji, Y., Xu, K., Li, Y., Wicks, K., Liu, J., Wong, K.W., Herman, I.M., Isberg, R.R., and Buchsbaum, R.J. (2010). Scaffold proteins IRSp53 and spinophilin regulate localized Rac activation by T-lymphocyte invasion and metastasis protein 1 (TIAM1). J. Biol. Chem. *285*, 18060–18071.

Roberts, A.W., Kim, C., Zhen, L., Lowe, J.B., Kapur, R., Petryniak, B., Spaetti, A., Pollock, J.D., Borneo, J.B., Bradford, G.B., et al. (1999). Deficiency of the hematopoietic cell-specific Rho family GTPase Rac2 is characterized by abnormalities in neutrophil function and host defense. Immunity *10*, 183–196.

Rossman, K.L., Der, C.J., and Sondek, J. (2005). GEF means go: turning on RHO GTPases with guanine nucleotide-exchange factors. Nat. Rev. Mol. Cell Biol. *6*, 167–180.

Sato, T., Vries, R.G., Snippert, H.J., van de Wetering, M., Barker, N., Stange, D.E., van Es, J.H., Abo, A., Kujala, P., Peters, P.J., and Clevers, H. (2009). Single Lgr5 stem cells build crypt-villus structures in vitro without a mesenchymal niche. Nature *459*, 262–265.

Timpson, P., McGhee, E.J., Morton, J.P., von Kriegsheim, A., Schwarz, J.P., Karim, S.A., Doyle, B., Quinn, J.A., Carragher, N.O., Edward, M., et al. (2011). Spatial regulation of RhoA activity during pancreatic cancer cell invasion driven by mutant p53. Cancer Res. *71*, 747–757.

Wang, X., He, L., Wu, Y.I., Hahn, K.M., and Montell, D.J. (2010). Light-mediated activation reveals a key role for Rac in collective guidance of cell movement in vivo. Nat. Cell Biol. *12*, 591–597.

Weiner, O.D., Marganski, W.A., Wu, L.F., Altschuler, S.J., and Kirschner, M.W. (2007). An actin-based wave generator organizes cell motility. PLoS Biol. *5*, e221.

Welch, H.C., Coadwell, W.J., Ellson, C.D., Ferguson, G.J., Andrews, S.R., Erdjument-Bromage, H., Tempst, P., Hawkins, P.T., and Stephens, L.R. (2002). P-Rex1, a PtdIns(3,4,5)P3- and Gbetagamma-regulated guanine-nucleotide exchange factor for Rac. Cell *108*, 809–821.

Welch, H.C., Condliffe, A.M., Milne, L.J., Ferguson, G.J., Hill, K., Webb, L.M., Okkenhaug, K., Coadwell, W.J., Andrews, S.R., Thelen, M., et al. (2005). P-Rex1 regulates neutrophil function. Curr. Biol. *15*, 1867–1873.

Wennerberg, K., Rossman, K.L., and Der, C.J. (2005). The Ras superfamily at a glance. J. Cell Sci. *118*, 843–846.

Xu, H., Kardash, E., Chen, S., Raz, E., and Lin, F. (2012). Gβγ signaling controls the polarization of zebrafish primordial germ cells by regulating Rac activity. Development *139*, 57–62.

Yagi, S., Matsuda, M., and Kiyokawa, E. (2012a). Chimaerin suppresses Rac1 activation at the apical membrane to maintain the cyst structure. PLoS ONE *7*, e52258.

Yagi, S., Matsuda, M., and Kiyokawa, E. (2012b). Suppression of Rac1 activity at the apical membrane of MDCK cells is essential for cyst structure maintenance. EMBO Rep. *13*, 237–243.

Yoshizaki, H., Ohba, Y., Kurokawa, K., Itoh, R.E., Nakamura, T., Mochizuki, N., Nagashima, K., and Matsuda, M. (2003). Activity of Rho-family GTPases during cell division as visualized with FRET-based probes. J. Cell Biol. *162*, 223–232.